Vertical Beamwidth Optimization of 3D-BF Pico-BS in mmWave HetNets

Naoto Inagaki and Takatoshi Sugiyama

Graduate School of Engineering, Kogakuin University, 1-24-2, Shinjuku-ku, Tokyo, 163-8677 Japan e-mail: cm24009@ns.kogakuin.ac.jp

Abstract—By incorporating picocells operating in the millimeter-wave (mmWave) bands into heterogeneous mobile networks (HetNets), a wide bandwidth becomes available, thereby improving user throughput. Downlink three-dimensional beamforming (3D-BF) in HetNets is a promising technology for improving the received SINR at user equipment (UE). Previously, we have proposed a three-sector picocell equipped with 3D-BF for mmWave HetNets and have investigated its effectiveness in improving user throughput. In this paper, we discuss the vertical beamwidth optimization of 3D-BF pico-BS in mmWave HetNets from the perspective of user throughput. From the results of systemlevel computer simulations, when the vertical beamwidth of 3D-BF was 10 degrees, the average user throughput reached approximately 289 Mbps, providing the maximum average user throughput among the five patterns.

Keywords—HetNets, millimeter wave, 3D beamforming, vertical beamwidth, 1024-QAM, user throughput

I. INTRODUCTION

Heterogeneous mobile networks (HetNets) combine macrocells operated by high-power macro base stations (macro-BS) and picocells operated by low-power pico base stations (pico-BS), and are attracting attention as a promising method for increasing system capacity [1]–[3]. In terms of coexistence with different types of BSs, fifth-generation (5G) mobile systems operating in non-standalone mode (NSA) share the same structure as HetNets, meaning that 5G and fourth-generation (4G) BSs coexist in the same area [4]–[7].

In particular, HetNets using the millimeter wave (mmWave) picocells can provide higher user throughput due to the enormous available signal bandwidth of picocells [8]–[10]. However, mobile communications using mmWave suffer greater path loss compared to conventional low-frequency bands in the free-space propagation loss models. Furthermore, mmWave signals are vulnerable to interference and obstruction caused by buildings and obstacles.

Downlink three-dimensional beamforming (3D-BF) at the BS improves the received signal-to-interference-plus-noise ratio (SINR) at the user equipment (UE) receiver and reduces interference to adjacent cells and other UEs through narrow beamwidths [11],[12]. Furthermore, the use of 3D-BF technology in the mmWave is effective in significantly improving the drawback of high propagation loss.

In [13]–[15], we have proposed sectorized pico-BS equipped with 3D-BF in mmWave HetNet, and have investigated the effectiveness from the user throughput points of view using computer simulations. Until now, we have evaluated the vertical beamwidth of 3D-BF in mmWave pico-BS with a fixed value of 10 degrees. Therefore, performance evaluation when changing the vertical beamwidth in mmWave pico-BSs equipped with 3D-BF has not yet been examined.

With this background, we investigate the vertical beamwidth optimization of 3D-BF pico-BS in mmWave HetNets, as parameters of the vertical beamwidth for mmWave pico-BS. Specifically, using system-level computer simulations, we clarify the average and 5-percentile user throughputs of mmWave HetNets composed of three-sector picocells equipped with 3D-BF versus five patterns of vertical beamwidth.

Section II describes an overview of three-sector picocells equipped with 3D-BF in mmWave HetNets. In Section III, we first describe the vertical beamwidth of the pico-BS equipped with 3D-BF. Then, we demonstrate the average and 5-percentile user throughput of mmWave HetNets for five patterns of vertical beamwidth of 3D-BF in mmWave pico-BS. Additionally, we analyze the use rate of each modulation method used in the downlink MCS and CDF characteristics of received SINR, SNR, and SIR. Section IV concludes our work.

II. THREE-SECTOR PICO-BS EQUIPPED WITH 3D-BF

Figure 1 shows a mmWave HetNet combining macrocells using the 2 GHz band for macro-BS and picocells using the 28 GHz band for pico-BS. The number of macro-sectors and picosectors is fixed to 3. In general, the cell selection is based on the measurement results of the downlink reference signal received power (RSRP) or the received signal-to-interference-plus-noise ratio (SINR) for both the macro-BS and pico-BS. The UEs basically connect to the cell with the highest measured downlink RSRP.

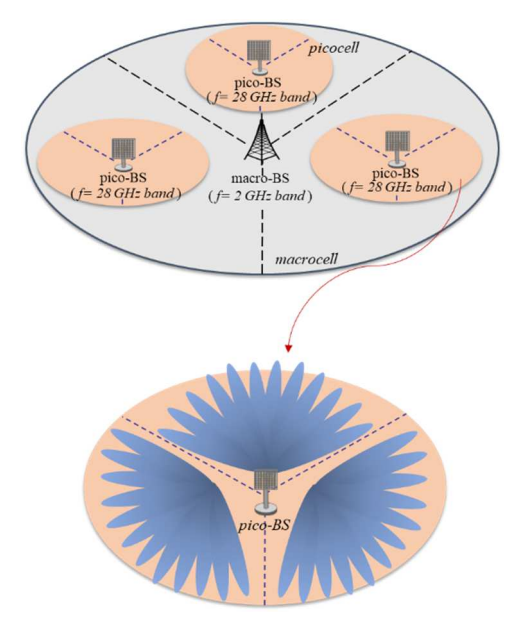


Fig. 1. Three-sector pico-BS equipped with 3D-BF in mmWave HetNet.

The bottom part of Fig. 1 shows a three-sector pico-BS, with each sector capable of forming up to 12 Tx beams in the azimuth plane. Furthermore, the number of Tx beams available in the elevation plane is fixed at 3. Therefore, the total number of Tx beams in each picocell sector is 36, obtained by combining the azimuth and elevation directions.

Figure 2 illustrates the beam selection procedure of the optimal beam among available beams. First, the pico-BS sequentially transmits the reference signals (RSs) for each beam to the UE. The UE measures the received RS and reports the channel state information (CSI) to the pico-BS. Based on the reported CSI, the pico-BS selects the optimal Tx beam for the UE among available beams. Subsequently, the pico-BS and UE communicate using the Tx beam. The CSI also includes the channel quality indicator (CQI), which is used to determine the modulation and coding scheme (MCS) for the downlink.

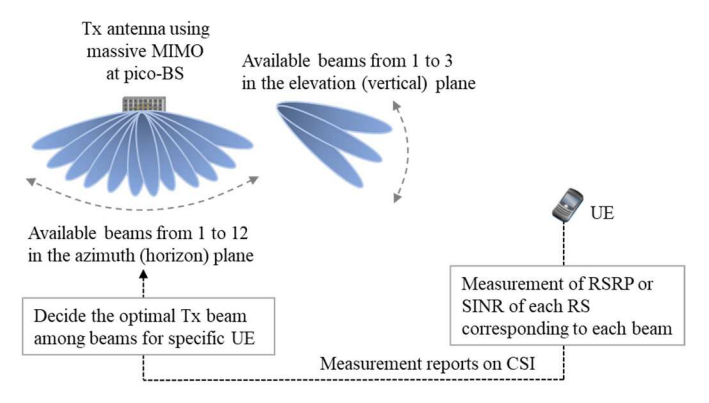


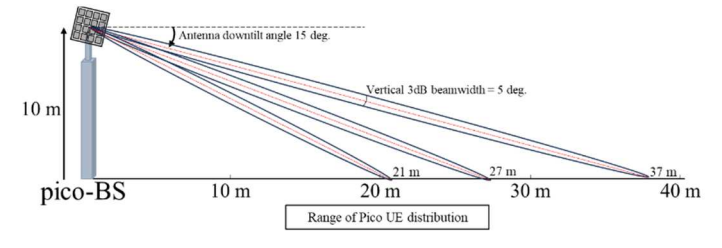
Fig. 2. Beam selection procedure between pico-BS and UE.

III. SIMULATION CONDITIONS AND RESULTS

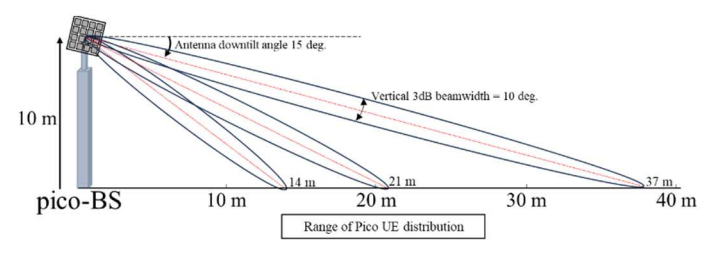
A. Vertical Beamwidth Difference in pico-BSs with 3D-BF

Figures 3-(a) to (e) show the vertical beamwidth of a three-sector pico-BS equipped with 3D-BF. When the vertical beamwidth is changed, the ground reach distance of the Tx beam radiated from the base station changes. For the three vertical beams, the uppermost beam is radiated based on an antenna down-tilt angle of 15 degrees, so the ground reach distance remains unchanged at 37 m for all five patterns.

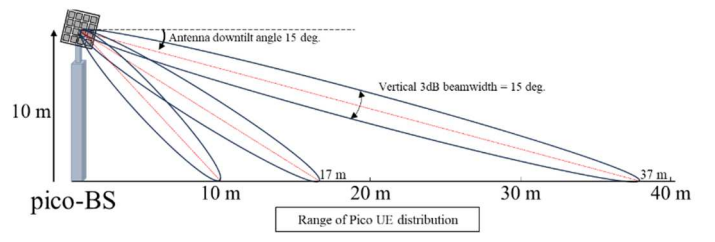
However, as the beamwidth widens, the ground reach distance from the base station for the middle and lowest beams shortens accordingly.



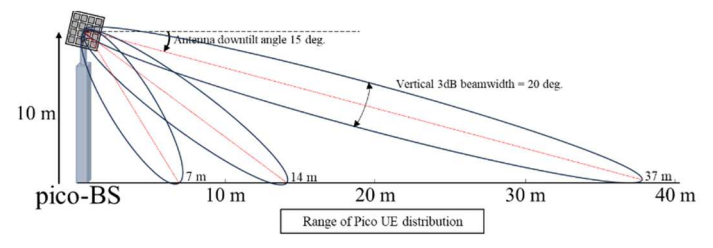
(a) Pattern I



(b) Pattern II



(c) Pattern III



(d) Pattern IV

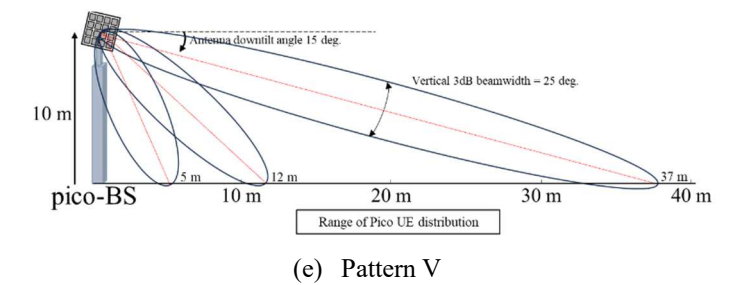


Fig. 3. Vertical beamwidth of 3D-BF Pico-BS

B. Simulation Parameters

The primary simulation parameters are shown in Table I. The carrier frequencies used in the macro- and pico-BSs are 2 and 28 GHz, respectively. The system bandwidth of the macro- and pico-BSs are assumed to be 10 and 100 MHz, respectively. The height of the pico-BS is set to 10 m [17]. The transmission method uses 2×2 single-user MIMO (SU-MIMO). Each UE is equipped with two receiving antennas. The number of UEs is fixed to be 30 per macro-sector. The UE are distributed on the rule of a cluster distribution in which 2/3 of the number of UE are placed nearby the pico-BSs and the rest are uniformly placed within the macro-BS. Link adaptation is applied to the downlink signal according to the received SINR at the UE receiver. We use 32 different types of MCS indexes for the link adaptation [14]–[16], where the modulation method is QPSK to 1024-QAM.

TABLE I. PRIMARY SIMULATION PARAMETERS

Parameter		Assumption			
		macro-BS	pico-BS		
Cell layout		Hexagonal grid, 19 cell sites, 3 sectors per site	4 picos per macro-sector		
	Cell radius (ISD)	289 m (500 m)			
Carrier frequency band		2 GHz	28 GHz		
System bandwidth		10 MHz	100 MHz		
Number of Resource blocks		50	500		
Tx power		+46 dBm	+22 dBm		
Tx antenna height		32 m	10 m		
Antenna downtilt angle		15 deg.	15 deg.		
Link adaptation		32 MCS (QPSK to 1024-QAM)			
MIMO		2×2 SU-MIMO			
UE	Number of Rx antennas	2			
	Distribution	30 UEs per macro-sector, 2/3 clustered distribution			
	Rx antenna gain	0 dBi			
	Antenna height	1.5 m			
	Mobility	3 km/h			

Table II shows the value for the three-sector pico-BS equipped with 3D-BF. The three-sector pico-BS equipped with 3D-BF uses an array antenna with 64 antenna elements and a maximum Tx

antenna gain of 23 dBi, and the number of available Tx beams is 36 (H12×V3). In other words, by combining 12 different beams in the azimuth plane and 3 different beams in the elevation plane, 36 Tx beams can be generated. We analyze five patterns for the vertical beamwidths. Until now, we have evaluated three-sector pico-BS equipped with 3D-BF by fixing the vertical beamwidth at 10 degrees. Pattern II in Table II corresponds to this. And, we will add four new patterns for evaluation. Pattern I has a vertical beamwidth of 5 degrees, and we will evaluate five vertical beamwidths at 5-degree intervals.

TABLE II. PARAMETERS OF THREE-SECTOR PICO-BS EQUIPPED 3D-BF

Parameter		Assumption of three-sector pico-BS equipped with 3D-BF					
Pattern		I	II	III	IV	V	
Tx Antenna	64 antenna elements						
Max. Tx antenna gain		23 dBi 5+10log(64)=5+18=23					
Beam numbers per sector (Horizontal × Vertical)		36 per sector, 12 beams in azimuth plane, and 3 beams in elevation plane					
Maximal attenuation	Horizontal	20 dB					
Maximal attenuation	Vertical	20 dB					
3dB beam width	Horizontal	10 deg.					
3db beam width	Vertical	5 deg.	10 deg.	15 deg.	20 deg.	25 deg.	

C. User Throughput

We investigated the user throughput in mmWave HetNets when using three-sector pico-BS equipped with 3D-BF as parameters of vertical beamwidths, i.e., for Patterns I, II, III, IV, and V. Figure 4 shows the average and 5-percentile user throughputs of mmWave HetNets. The blue and the orange bars show the user throughput for the average and that for the 5-percentile, respectively. Pattern II, i.e., when the vertical beamwidth of 3D-BF was 10 degrees, the average user throughput reached approximately 289 Mbps, which provided the maximum average user throughput among the five patterns. On the other hand, the 5-percentile user throughput improved as the vertical beamwidth of 3D-BF became wider.

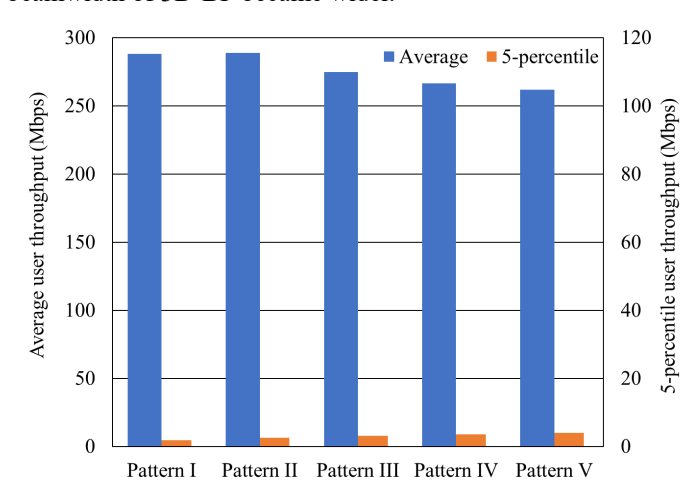


Fig. 4. Average and 5-percentile user throughput of mmWave HetNets.

Here, we analyze the performance in detail. The average user throughput deteriorates as the vertical beamwidth of 3D-BF widens, i.e., in the order of Pattern II, Pattern III, Pattern IV, and Pattern V. We consider that this is because the Tx gain decreased and the UE's received SINR declined due to the expansion of the vertical beamwidth of 3D-BF.

D. Analysis for use rate of 1024-QAM

Figure 5 analyzes the use rate of each modulation method used in the downlink MCS[14]–[16]. It can be seen that Pattern II improves the use rate of 1024-QAM and reaches approximately 54%. This must be one reason that Pattern II provides the best average user throughput among the five patterns, as shown in Fig. 4.

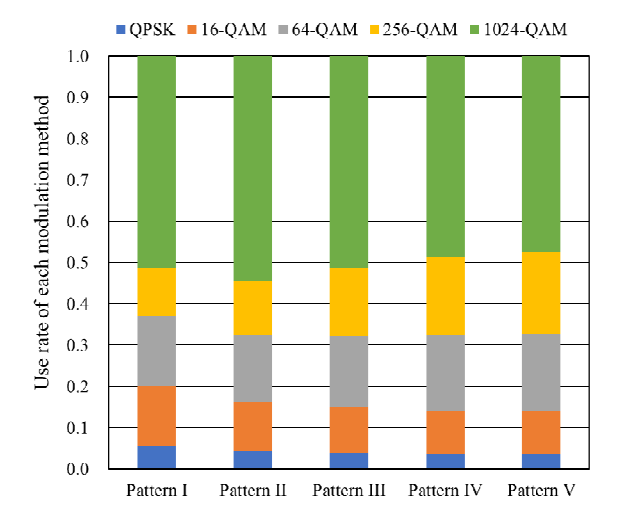


Fig. 5. Use rate of each modulation method used in downlink MCS.

E. CDF characteristics of received SINR, SNR, and SIR

Figure 6 analyzes the CDF characteristics of received SINR. The received SINR of Pattern II at CDF=0.5 is approximately 28 dB, which is the maximum value among the five patterns. Similar to the result in Fig. 5, this result also suggests that Pattern II provides the best average user throughput among the five patterns, as shown in Fig. 4.

However, a reversal in values was observed around CDF=0.3 to 0.4. In order to identify the cause of this phenomenon, we analyzed the CDF characteristics of the received SNR and SIR as shown in Figures 7 and 8. In Fig. 8, the values are reversed in the same way as the CDF characteristics of the received SINR in Fig. 6. However, in the CDF characteristics of the SNR in Fig. 7, the values are not reversed. That is, the cause of the reversal of the received SINR values is considered to be interference.

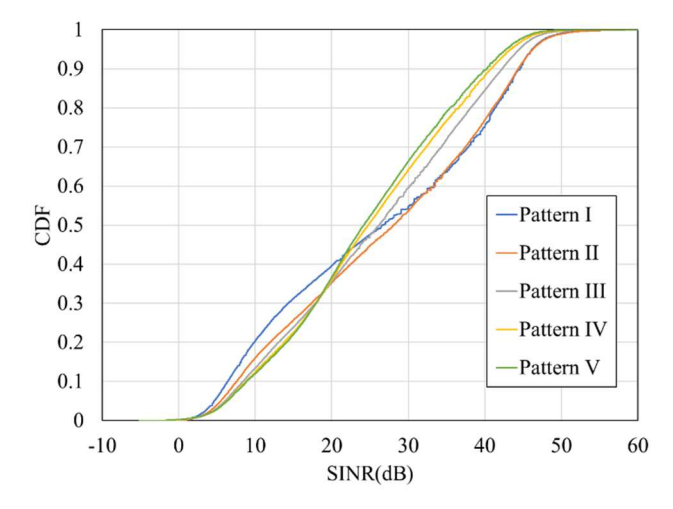


Fig. 6. CDF of received SINR of mmWave HetNets.

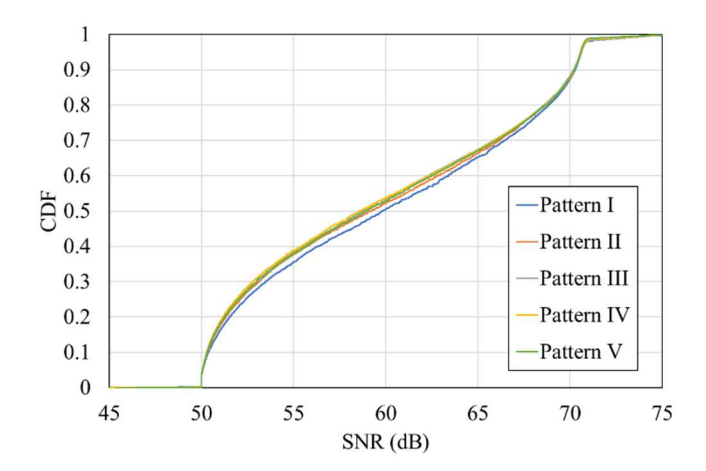


Fig. 7. CDF of received SNR of mmWave HetNets.

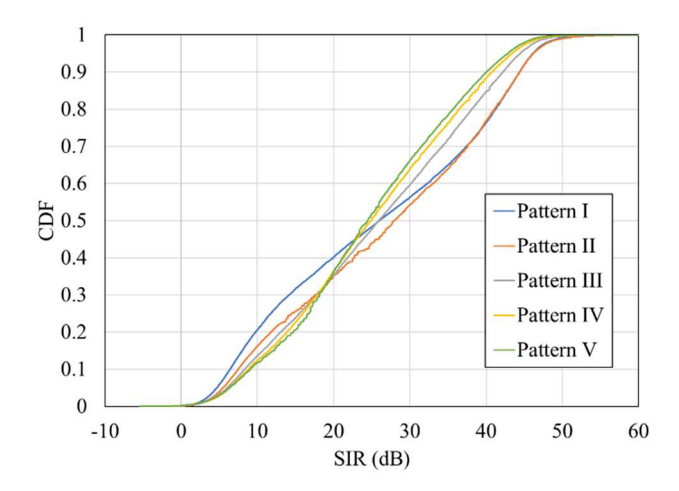


Fig. 8. CDF of received SIR of mmWave HetNets.

IV. CONCLUSION

In this paper, we investigated the vertical beamwidth optimization of 3D-BF pico-BS in mmWave HetNets from the perspective of user throughput. Specifically, we evaluated the average and 5-percentile user throughput of HetNets against five patterns of vertical beamwidth of 3D-BF in mmWave pico-BS, using system-level computer simulations. From these results, Pattern II with a vertical beamwidth of 10 degrees provided the best performance among the five patterns. In addition, we considered that if the vertical beamwidth is too wide, it deteriorates the average user throughput due to a decrease in the UE's received SINR caused by a decline in Tx gain. As a future work, we are planning to extend our analysis to different UE distributions and mobility conditions.

ACKNOWLEDGMENT

The authors would like to express his deep gratitude to Prof. Hiroyuki Otsuka for his guidance.

REFERENCES

- I. Guvene, "Capacity and Fairness Analysis of Heterogeneous Networks with Range Expansion and Interference Coordination," *IEEE Commun. Letters*, vol. 15, issue 10, Oct. 2011.
- [2] K. Kikuchi and H. Otsuka, "Proposal of Adaptive Control CRE in Heterogeneous Networks," in Proc. PIMRC2012, pp. 910-914, Sept. 2012.
- [3] E. Dahlman, K. Dimou, S. Parkvall, and H. Tullberg, "Future wireless access small cells and heterogeneous deployments," in *Proc. ICT*, May 2013.
- [4] D. Soldani and A. Manzalini, "Horizon 2020 and Beyond: On the 5G Operating System for a True Digital Society," *IEEE Veh. Tech. Mag.*, vol. 10, no. 1, pp. 32-42, March 2015.
- [5] T. E. Bogale and L. B. Le, "Massive MIMO and mmWave for 5G Wireless HetNet: Potential Benefits and Challenges," *IEEE Veh. Tech. Mag.*, vol. 11, no. 1, pp. 64-75, March 2016.
- [6] 3GPP TR 23.501, "System Architecture for the 5G System (5GS)," Release 15, June 2018.
- [7] B. Cai, H. Zhang, H. Guo, G. Zhang, and W. Xie, "5G Network Evolution and Dual-mode 5G Base Station," in *Proc. 6th ICCC*, pp. 283-277, Dec. 2020
- [8] R. Baldemair, T. Irnich, K. Balachandran, E. Dahlman, G. Mildh, Y. Selen, S. Parkvall, M. Meyer, and A. Osserian, "Ultra-dense networks in millimeter-wave frequencies," *IEEE Commun. Mag.*, vol. 53, no. 1, pp. 202-208, Jan. 2015.
- [9] T. S. Rappaport, S. Sun, R. Mayzus, H. Zhao, Y. Azar, K. Wang, G. N. Wong, J. K. Schulz, M. Samimi, F. Gutierrez, "Millimeter Wave Mobile Communications for 5G Cellular: It Will Work!", *Access IEEE*, vol. 1, pp. 335-349, May 2013.
- [10] M. Xiao, S. Mumtaz, Y. Huang, L. Dai, Y. Li, M. Matthaiou, G. Karagiannidis, E. Bjornson, K. Yang, C-L. I, and A. Ghosh, "Millimeter Wave Communications for Future Mobile Networks," *IEEE J. Sel. Areas Commun.*, vol. 35, no. 9, pp. 1909-1935, Sept. 2017.
- [11] 3GPP TSG RAN WGI #86, "Beam Management Procedure for NR MIMO," Aug. 2016.

- [12] Y. Song, X. Yun, S. Nagata, and L. Chen, "Investigation on elevation beamforming for future LTE-Advanced," in *Proc. ICC2013 Workshop Beyond LTE-A*, pp.106-110, June 2013.
- [13] Y. Omura, F. Kemmochi, K. Fujisawa, and H. Otsuka, "Implementation of MCS Incorporating 1024-QAM and Beam-Based Transmission in 3D-BF," in *Proc. VTC2020-Spring*, 1D-2, May 2020.
- [14] N. Inagaki, K. Yoda, T. Yasaka, S. Suyama, and H. Otsuka, "Impact of 3D-BF against the Number of Picocell Sector in mmWave HetNets," in *Proc. APWCS2023*, pp. 1-5, August 2023.
- [15] N. Inagaki, S. Suyama, and H. Otsuka, "Impact of Twelve-Sector Picocells with 3D-BF in mmWave HetNets," in Proc. APWCS2024, pp. August 2024.
- [16] N. Inagaki, S. Suyama, and H. Otsuka, "A Study on the Layout of mmWave Pico-BS with 3D-BF," in Proc. *IEICE General Conference*—2025, March 2025 (in Japanese).
- [17] N. Inagaki, T. Sugiyama, "Optimization of Base Station Height in mmWave Pico-BS equipped with 3D-BF," in Proc. *IEICE Society Conference*—2025, September 2025 (in Japanese).